ARL-TN-1097 ● Dec 2021

DEVCOM ARMY RESEARCH LABORATORY

Small-Angle X-ray Scattering Analysis of Morphology in 7075 Aluminum

by Frederick L Beyer and Daniel J Magagnosc

NOTICES

Disclaimers

The findings in this report are not to be construed as an official Department of the Army position unless so designated by other authorized documents.

Citation of manufacturer's or trade names does not constitute an official endorsement or approval of the use thereof.

Destroy this report when it is no longer needed. Do not return it to the originator.

ARL-TN-1097 ● DEC 2021

Small-Angle X-ray Scattering Analysis of Morphology in 7075 Aluminum

Frederick L Beyer and Daniel J Magagnosc
Weapons and Materials Research Directorate,
DEVCOM Army Research Laboratory

REPORT DOCUMENTATION PAGE

Form Approved
OMB No. 0704-0188

1. REPORT DATE *(DD-MM-YYYY)*	2. REPORT TYPE	3. DATES COVERED (From - To)
December 2021	Technical Note	1 June–31 August 2021

4. TITLE AND SUBTITLE
Small-Angle X-ray Scattering Analysis of Morphology in 7075 Aluminum

5a. CONTRACT NUMBER

5b. GRANT NUMBER

5c. PROGRAM ELEMENT NUMBER

6. AUTHOR(S)
Frederick L Beyer and Daniel J Magagnosc

5d. PROJECT NUMBER

5e. TASK NUMBER

5f. WORK UNIT NUMBER

7. PERFORMING ORGANIZATION NAME(S) AND ADDRESS(ES)
DEVCOM Army Research Laboratory
ATTN: FCDD-RLW-MG
Aberdeen Proving Ground, MD 21005

8. PERFORMING ORGANIZATION REPORT NUMBER
ARL-TN-1097

9. SPONSORING/MONITORING AGENCY NAME(S) AND ADDRESS(ES)

10. SPONSOR/MONITOR'S ACRONYM(S)

11. SPONSOR/MONITOR'S REPORT NUMBER(S)

12. DISTRIBUTION/AVAILABILITY STATEMENT
Approved for public release: distribution unlimited.

13. SUPPLEMENTARY NOTES
ORCID ID(s): Frederick L Beyer, 0000-0003-0253-2134; Daniel J Magagnosc, 0000-0002-1418-9292

14. ABSTRACT
A small-angle X-ray scattering (SAXS) study of heat-treated aluminum (Al) alloy 7075 was performed. Samples were annealed for different periods of time, then characterized using SAXS. The microstructure contains two nanoscale precipitate types as confirmed via electron microscopy: roughly 5-nm precipitates produced during heat treatment and roughly 60-nm precipitates primarily generated during quenching. The size and number of the smaller precipitates were found to increase with annealing time, although annealing samples 4 h resulted in a drop in the volume fraction of small precipitates. This effort demonstrates the applicability of SAXS to heat-treatment development in Al alloys.

15. SUBJECT TERMS
small-angle X-ray scattering, SAXS, aluminum, 7075, precipitate, morphology

16. SECURITY CLASSIFICATION OF:			17. LIMITATION OF ABSTRACT	18. NUMBER OF PAGES	19a. NAME OF RESPONSIBLE PERSON
a. REPORT	b. ABSTRACT	c. THIS PAGE			Frederick L Beyer
Unclassified	Unclassified	Unclassified	UU	21	19b. TELEPHONE NUMBER (Include area code) (410) 306-0893

Contents

List of Figures

Acknowledgments

The authors thank Heather Murdoch for assistance in calculating the density of the $MgZn_2$ phase.

1. Introduction

Aluminum (Al) alloy 7075 (AA7075) is a precipitation-strengthened Al alloy in which the primary alloying elements are zinc and magnesium.[1] Known for its high strength, the mechanical properties of AA7075 (i.e., strength, fracture toughness, and ductility) are controlled via various annealing and aging processes. Although AA7075 was developed for aerospace applications, recently specific AA7075 tempers have been qualified for ballistic applications in plates up to 1.5 inches thick.[2] The sensitivity of mechanical properties to tempering procedures leads to challenges in developing the correct heat-treatment protocol for a given application. The strength and ductility of AA7075 is largely a function of nanoscale $MgZn_2$ η/η' precipitates with sizes on the order of 5 to 10 nm.[3,4] These precipitates are produced during final aging treatments. However, the failure properties are affected by larger (50 to 250 nm) $MgZn_2$ precipitates formed before aging.[5,6] These larger precipitates act as nucleation sites for voids, leading to fracture.

Experimental verification of the various precipitates is critical to the development of tempers and in validating process modeling, but conventional characterization relies on time-consuming transmission electron microscopy. Small-angle X-ray scattering (SAXS) offers an alternative route to quantitative and statistically significant measurements of nanoscale precipitates. SAXS is a nondestructive bulk measurement technique similar to powder X-ray diffraction.[7] In a typical SAXS experiment, a highly collimated beam of photons is transmitted through a thin sample. The scattered X-rays are measured at a relatively large distance (typically 1–2 m) as a function of angle. The scattered X-rays contain information about the size and shape of the scattering domain or object, and if the data are collected on a calibrated intensity scale, information about domain or object quantity can also be extracted.

In this study, AA7075 plates subject to different aging treatments have been examined to determine the size, shape, and volume fraction of precipitates. This report provides the results of SAXS characterization of a series of AA7075 samples annealed for different amounts of time.

2. Experimental

2.1 Materials

Four AA7075 samples subjected to different aging treatments were prepared for SAXS measurements. Thin sections were cut from a 30-mm-thick plate and then ground to approximately 100 μm thickness. Discs 3 mm in diameter were punched

out of the thin sections and further ground to a final thickness of approximately 50 μm, suitable for SAXS characterization. The four samples were AA7075-T651 and were subjected to different-length final-aging steps. They were annealed at 180 °C for 0 (control sample), 2, 3, and 4 h.

2.2 Small-Angle X-ray Scattering (SAXS)

SAXS data were collected using a Xenocs (Grenoble, France) "Xeuss 3.0 HR" instrument with 8.04 keV photons generated by a Rigaku (The Woodlands, Texas) 007HF rotating anode X-ray generator. The photons were collimated using a focusing optic and two scatterless slit apertures, producing a well-aligned incident beam with wavelength, λ, of 1.5418 Å. Data were collected using a Dectris (Dättwil, Switzerland) PILATUS3 R 300K hybrid-pixel detector at two sample-to-detector distances, 1800 and 900 mm, to give a combined angular range of $0.003\ \text{Å}^{-1} < q < 0.3\ \text{Å}^{-1}$, where q is the modulus of the scattering vector, such that $q = 4\pi \sin(\theta)/\lambda$, where 2θ is the scattering angle. 2-D data were azimuthally averaged to generate 1-D data, $I(q)$, for analysis. The instrument configuration was calibrated using silver behenate,[8] data were placed on an absolute scale as described in the following, and corrected for instrumental artifacts and noise.[9]

The solid-state design of the Pilatus detector allows very accurate conversion of data from arbitrary units to absolute intensity (units of cm^{-1}), a step that is important for quantitative analysis of SAXS data.[9] Equation 1 gives the measured intensity, $I_S(q)$, as a function of source flux (J_0, cts/s), time (t, s), illuminated area (A), sample thickness (d), solid angle ($\Delta\Omega$), detector efficiency ($\eta(\lambda)$), sample transmission, T_d, and the differential scattering cross-section function ($d\sigma/d\Omega$) that describes the internal structure of the material.

$$I_S(q) = J_0 \cdot t \cdot A \cdot d \cdot \Delta\Omega \cdot \eta(\lambda) \cdot T_d \cdot \frac{d\sigma(\mathrm{q})}{d\Omega} \tag{1}$$

Sample transmission describes the amount of the incident beam that is transmitted through the sample and is a function of the linear absorption coefficient (μ) and sample thickness, as given by Eq. 2. The linear absorption coefficient for Al at 8 keV is 136 cm^{-1}, leading to an optimum sample thickness of 80 μm.

$$T_d = \frac{J_d}{J_0} = e^{-\mu d} \tag{2}$$

Because the Pilatus detector allows the measurement of the direct beam intensity, $I(0)$, one can obtain J_d, the transmitted flux, and then replace J_0 and T_d in Eq. 1. All the other quantities are known, allowing the data to be placed on an absolute scale. The same process is used for the empty cell data, allowing subtraction of instrumental artifacts from the measured sample data. This process was

independently verified using calibrated glassy carbon as a secondary intensity standard.[10] The differential scattering cross-section determined in a small-angle scattering experiment will be denoted $I(q)$ from this point forward.

2.3 Data Analysis

Data reduction was performed using Wavemetrics (Lake Oswego, Oregon) Igor Pro v8 and procedures available for download from Argonne National Laboratory.[11] Data analysis was also performed using Igor Pro v8 with a separate set of procedures from Argonne National Laboratory.[12] In the analysis, a model function was fit to the data and then optimized using a linear least-squares approach. The data reported here were obtained by fitting model functions having a log-normal distribution of radii (e.g., precipitate radius). Reported standard deviations are fractional.

3. Results

The scattered intensity from materials containing two or more phases is the product of two terms—one describing the shape of the minority component and one describing the spatial arrangement of the minority component, as given in Eq. 3. These two terms are the form factor, $P(q)$, and structure factor, $S(q)$, respectively. When the minority phase is diluted, so that the scattering from different particles or domains does not interfere with that from other particles or domains, only the form factor, $P(q)$, need be considered in the analysis. Furthermore, the form factor scattering is the square of the scattering amplitude, $B(q)$.[7]

$$I(q) \propto P(q)S(q) \propto B^2(q) \cdot 1 \tag{3}$$

The scattering amplitude function is effectively the origin of X-ray scattering in a material and is simply the Fourier transform of the scattering length density, ρ, throughout the particle and relative to the average scattering length density throughout the sample, ρ_0, as given in Eq. 4. Here r is the correlation length in real space and ρ_0 is the mean scattering length density throughout the sample.[13]

$$B(q) = 4\pi \int_0^\infty [\rho(r) - \rho_0] \frac{\sin qr}{qr} r^2 dr \tag{4}$$

Exact analytical expressions for $B(q)$ exist only for a few shapes, such as the form factor amplitude for a homogenous spherical particle (Eq. 5).[14] Equation 6 provides the solution for a cylindrical domain, where B_1 is the first-order Bessel function, R is radius, L is length, and α is the angle between the cylinder axis and the incident beam.[15]

$$B(q,R) = \frac{3[\sin(qR) - qR\cos(qR)]}{(qR)^3} \tag{5}$$

$$B(q,R,L) = \int_0^{\pi/2} \left[\frac{2B_1(qR\sin(\alpha))}{qR\sin(\alpha)} \frac{\sin((qL\cos(\alpha)/2)}{(qL\cos(\alpha)/2)}\right]^2 \sin(\alpha) d\alpha \tag{6}$$

Additionally, the radius of gyration (R_g) of a particle is often calculated as a means of quickly assessing particle size. It is analogous to the radius of inertia in mechanics. Equation 7 gives the relationship between R_g and R for a sphere and Eq. 8 gives the relationship between R_g, R, and L for a cylinder.[16]

$$R_g = \sqrt{\frac{3}{5}R^2} \tag{7}$$

$$R_g = \sqrt{\frac{R^2}{2} + \frac{L^2}{12}} \tag{8}$$

The SAXS data collected for the four samples are presented in Fig. 1. All four samples show evidence of Guinier scattering (form factor scattering) from particles or domains having a relatively broad size distribution. The Guinier scattering is most evident in the control sample (red circles), with a pronounced Guinier "knee" at approximately 0.1 Å^{-1}. Upon annealing, this feature shifts to lower angles (larger sizes) and becomes less pronounced, suggesting that the particles or domains become larger but also more size diverse.

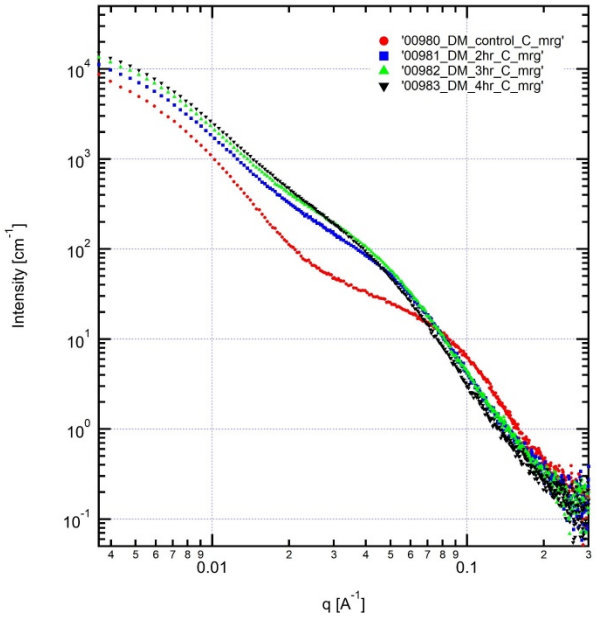

Fig. 1 SAXS data collected for the four Al samples provided

Figure 2 shows the results of using least-squares fitting of a model to the data for the control sample. The model consists of two contributions other than a constant background (fixed at 0.2 cm^{-1})—one for the small domains having Guinier scatter

clearly visible at 0.1 $Å^{-1}$ and a second for a larger particle or domain exhibiting Guinier scattering at lower angles, centered around 0.006 $Å^{-1}$. The model function after fitting to the data is shown in green. The parameters of the two form factors are appended to the graph and show that the small domains have $R_g \approx 26$ Å, while the large domains have an $R_g \approx 294$ Å. The smaller domains have a narrower size distribution (as described by the full width at half maximum). The fractional standard deviations for the log-normal distribution of radii are 0.34 (smaller domains) and 0.54 (larger domains), indicating significant variation in radius for both sizes of domains.

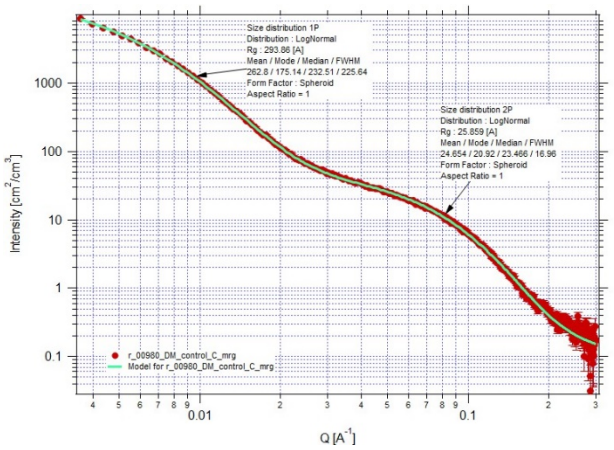

Fig. 2 Results of least-squares fitting of a simple form factor model function to the data for the control sample

Figure 3 shows the fit of the same model function to the data for the sample annealed 2 h. The small domains have increased in size to $R_g \approx 44$ Å, while the large domains have decreased to $R_g \approx 260$ Å. The breadth of the size distribution for the smaller domains has also increased substantially, with standard deviation increasing to 0.40.

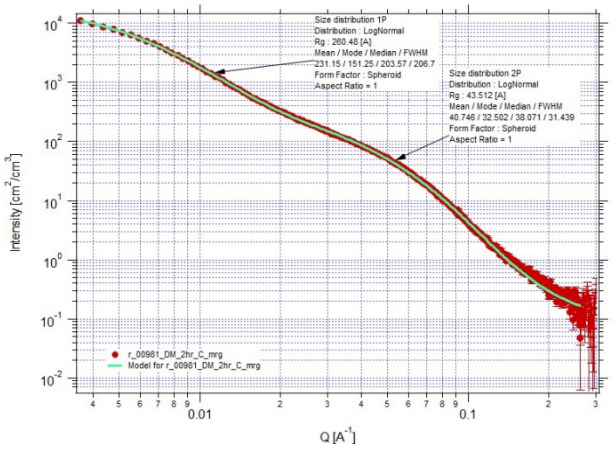

Fig. 3 Results of fitting form factor model function to SAXS data for sample annealed 2 h

Figures 4 and 5 show the results of fitting the form factor model function to the SAXS data collected for the samples annealed 3 and 4 h, respectively. The size of the smaller domains continues to increase with annealing time to 51 and 57 Å, respectively, with fractional standard deviations of 0.44 and 0.46.

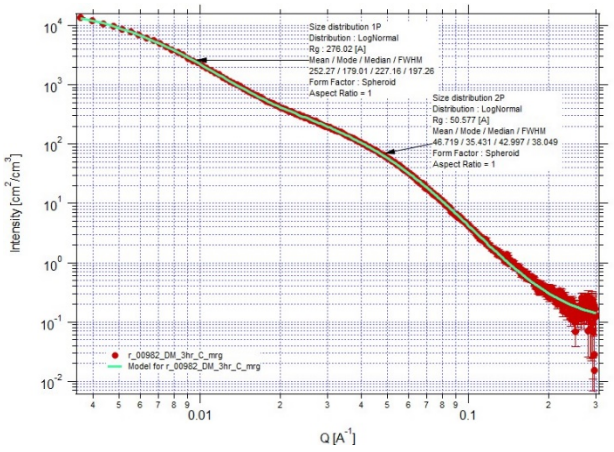

Fig. 4 Results of least-squares fitting of model to data for sample annealed 3 h

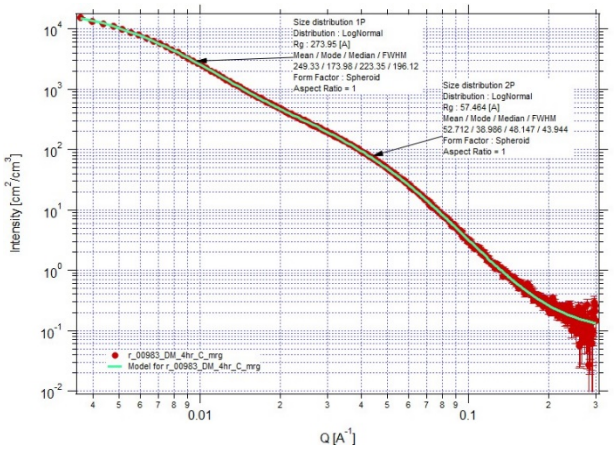

Fig. 5 Results of least-squares fitting of model to data for sample annealed 4 h

The results of fitting a model to the data for the larger domains, at lower scattering angle, are somewhat speculative. More confidence in the specific results is only possible if data could be collected at angles lower than 0.003 Å^{-1}.

Figures 6 and 7 show the results of fitting the data using a model that combines the form factor for a sphere for the large domains (low q) and the form factor for cylinders for the small domains (high q). By constraining the cylindrical form factor so that length is less than radius, a disc-like particle shape is generated.

Figure 6 shows the results of the least-squares fit of the model using a cylindrical form factor to incorporate a disc shape for the smaller particles. The fit is generally

good and results in a disc having R_g of 31 Å, mean radius of 30.6 Å, and length (thickness) of 28.3 Å.

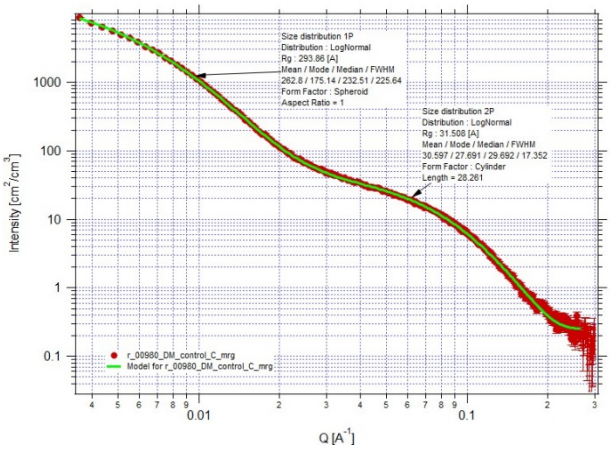

Fig. 6 Fit of model including disc-shaped particle for high q scattering for the control sample

Figures 7–9 all show very similar results for model fits to the scattering data. The disc-shaped smaller domains increase in size after annealing to have R_g of approximately 60 Å, radii of approximately 58 Å, and lengths ranging from 41 Å (2-h anneal) to 47 Å (4-h anneal). The increase in size shifts the form factor scattering to lower angles and reveals the first form factor "fringe", around 0.2 Å^{-1}. In general, increased size dispersity smooths such fringes out into a power-law decrease in scattered intensity, with $I(q)$ scaling as q^{-4} (Porod Law scattering).[7] Here, however, the model fit is constrained to fit the higher intensity, lower error data between 0.02 and 0.1 Å^{-1}, resulting in a model fit that retains the form factor fringe. Relaxing that constraint leads to large errors in the fit at lower angles and is thus not valid. These results suggest the domains may change shape from discotic to spherical as they grow during the annealing process, or that they may be spherical even in the control sample.

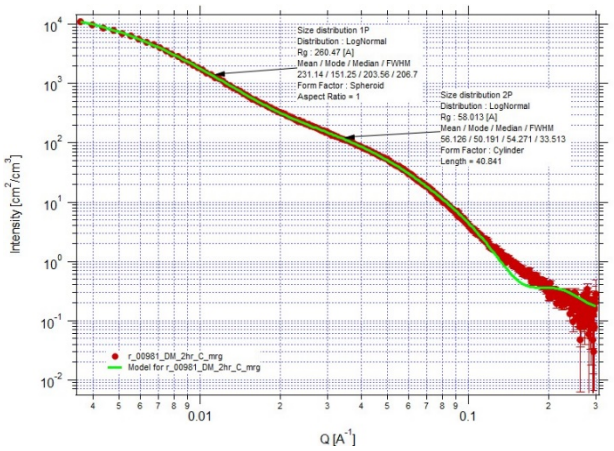

Fig. 7 Fit of model including disc shape for smaller particles for the sample annealed 2 h

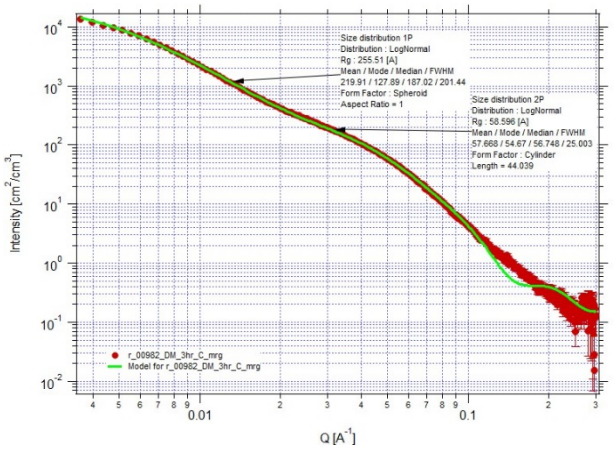

Fig. 8 Fit of model including disc shape for smaller particles for the sample annealed 3 h

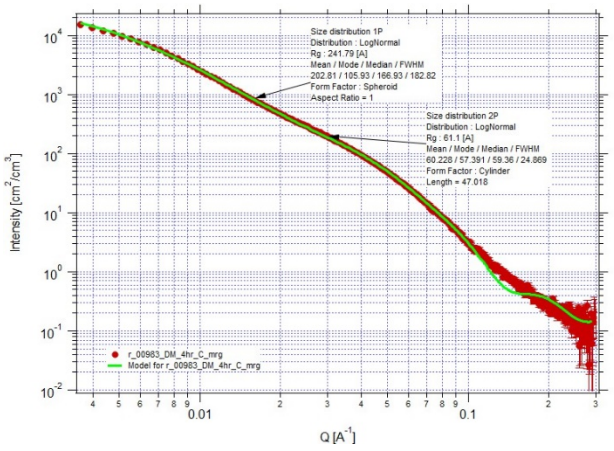

Fig. 9 Fit of model including disc shape for smaller particles for the sample annealed 4 h

Placing the data on an absolute intensity scale allows the volume fraction of the different components to be extracted, where the contrast between components can be calculated. In this case, the density of the Al alloy matrix was calculated to be

2.6999 g·cm^{-3}, while the density of the smaller precipitates was calculated to be 5.7596 g·cm^{-3}, giving an extremely large X-ray contrast value of 535 × 10^{20} cm^{-4}. With such a high contrast, it was expected that the volume fractions of the precipitates would be low.

Figure 10 shows the volume fractions of the small precipitates for the four different samples. The values differ slightly between the model fits using a sphere form factor and a disc form factor (a cylinder with length << diameter). Both analyses show increasing volume fractions with increasing annealing time, but then a sharp drop for the sample annealed 4 h. In all cases, the volume fractions are on the order of 1%, reflecting the high density of the precipitate relative to the matrix.

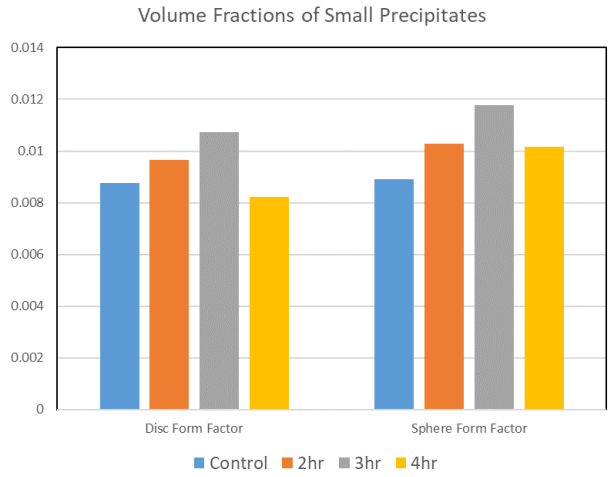

Fig. 10 Volume fractions of the small precipitate determined from the SAXS data for both the sphere model and disc model

The drop in volume fraction of precipitates from 3 h annealing to 4 h of annealing prompted a new experiment in which three different specimens from the sample annealed 4 h were characterized by SAXS. Figure 11 shows the SAXS data collected, along with the original data. No changes in the data were noted other than slight changes in intensity due to varying sample thicknesses, indicating that the drop in volume fraction is real.

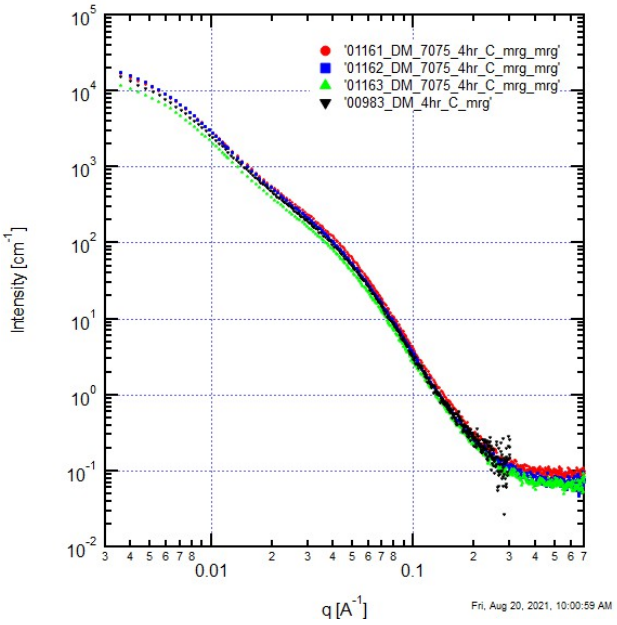

Fig. 11 SAXS data for three specimens of the sample annealed 4 h showing identical behavior

4. Conclusions

In this experiment, a series of AA7075-T651 Al alloy samples were annealed at 180° C for up to 4 h and then characterized using SAXS. Analysis of the SAXS data showed that the smaller precipitates increase in size with annealing time, from having an R_g of 26 Å in the control sample to 57 Å in the sample annealed 4 h. It was also noted in the analysis process that the model for a disc-shaped particle fit the data poorly, while the model for a spherical shape fit the data well. Finally, the content of the smaller precipitates was found to increase with annealing up to 3 h and then decrease on annealing to 4 h. This observation correlates well with observed softening due to over-aging. Overall, these results demonstrate the viability of characterizing nanoscale precipitates in aged Al alloys using laboratory-scale SAXS.

5. References

1. Anderson K, Weritz J, Kaufman JG, editors. 7075 and Alclad 7075: high-strength structural alloy. ASM International; 2019. p. 432–438. (ASM Handbook. Properties and selection of aluminum alloys; vol. 2B).

2. MIL-DTL-32375B, Amendment 3. Armor plate, aluminum alloy, 7085, 7056, 7075, and 7181, unweldable applique. Department of Defense (US); 2021 Jan 15.

3. Park JK, Ardell AJ. Microstructures of the commercial 7075 Al alloy in the T651 and T7 tempers. Metallurg Trans A. 1983;14(10):1957–1965.

4. Berg LK, Gjønnes J, Hansen V, Li XZ, Knutson-Wedel M, Waterloo G, Schryvers D, Wallenberg LR. GP-zones in Al-Zn-Mg alloys and their role in artificial aging. Acta Materialia. 2001;49(17):3443–3451.

5. Broek D. A study on ductile fracture [doctoral thesis]. Delft University of Technology; 1971.

6. Broek D. The role of inclusions in ductile fracture and fracture toughness. Eng Fract Mech. 1973;5(1):55–66.

7. Roe R-J. Methods of X-ray and neutron scattering in polymer science. Oxford University Press; 2000.

8. Huang TC, Toraya H, Blanton TN, Wu YJ. X-ray powder diffraction analysis of silver behenate, a possible low-angle diffraction standard. J Appl Cryst. 1993;26:180–184.

9. Pauw BR. Everything SAXS: small-angle scattering pattern collection and correction. J Phys Condens Matter. 2013;25(38):383201.

10. Zhang F, Ilavsky J, Long GG, Quintana JPG, Allen AJ, Jemian PR. Glassy carbon as an absolute intensity calibration standard for small-angle scattering. Metall Mater Trans A. 2009;41(5):1151–1158.

11. Ilavsky J. Nika: software for two-dimensional data reduction. J Appl Cryst. 2012;45:324–328.

12. Ilavsky J, Jemian PR. Irena: tool suite for modeling and analysis of small-angle scattering. J Appl Cryst. 2009;42:347–353.

13. Seelenmeyer S, Deike I, Rosenfeldt S, Norhausen C, Dingenouts N, Ballauff M, Narayanan T, Lindner P. Small-angle X-ray and neutron scattering studies

of the volume phase transition in thermosensitive core-shell colloids. J Chem Phys. 2001;114(23):10471–10478.

14. Rayleigh L. The incidence of light upon a transparent sphere of dimensions comparable with the wave-length. Proc R Soc Lond A Math Phys. 1910;84(567):25–46.

15. Pedersen JS. Analysis of small-angle scattering data from colloids and polymer solutions: modeling and least-squares fitting. Adv Colloid Interface Sci. 1997;70:171–210.

16. Kirste RG, Oberthur RC. Small angle X-ray scattering. In: Glatter O, Kratky O, editors. Academic Press; c1982. p. 387–431.

List of Symbols, Abbreviations, and Acronyms

1-D	one-dimensional
2-D	two-dimensional
AA7075	aluminum alloy 7075
Al	aluminum
ARL	Army Research Laboratory
DEVCOM	US Army Combat Capabilities Development Command
R_g	radius of gyration
SAXS	small-angle X-ray scattering

1 (PDF)	DEFENSE TECHNICAL INFORMATION CTR DTIC OCA
1 (PDF)	DEVCOM ARL FCDD RLD DCI TECH LIB
2 (PDF)	DEVCOM ARL FCDD RLW MG F L BEYER FCDD RLW MB D J MAGAGNOSC